Rapid microfluidic double-jump mixing device for single-molecule spectroscopy

Dingfelder, Fabian; Wunderlich, Bengt; Benke, Stephan; Zosel, Franziska; Zijlstra, Niels; Nettels, Daniel; Schuler, Benjamin

Abstract: We introduce a microfluidic double-jump mixing device for investigating rapid biomolecular kinetics with confocal single-molecule spectroscopy. This device enables nonequilibrium dynamics to be probed, e.g., transiently populated intermediates that are inaccessible with existing single-molecule approaches. We demonstrate the potential and reliability of the method on time scales from milliseconds to minutes by investigating the coupled folding and binding reaction of two intrinsically disordered proteins and the conformational changes occurring in a large cytolytic pore-forming toxin.

DOI: https://doi.org/10.1021/jacs.7b02357

Rapid Microfluidic Double-Jump Mixing Device for Single-Molecule Spectroscopy

Fabian Dingfelder*, Bengt Wunderlich*, Stephan Benke*, Franziska Zosel*, Niels Zijlstra*, Daniel Nettels* and Benjamin Schuler*,†,#

*Department of Biochemistry, University of Zurich, Winterthurerstrasse 190, 8057 Zurich, Switzerland
†Department of Physics, University of Zurich, Winterthurerstrasse 190, 8057 Zurich, Switzerland

Supporting Information Placeholder

ABSTRACT: We introduce a microfluidic double-jump mixing device for investigating rapid biomolecular kinetics with confocal single-molecule spectroscopy. This device enables non-equilibrium dynamics to be probed, e.g. transiently populated intermediates that are inaccessible with existing single-molecule approaches. We demonstrate the potential and reliability of the method on timescales from milliseconds to minutes by investigating the coupled folding and binding reaction of two intrinsically disordered proteins and the conformational changes occurring in a large cytolytic pore toxin.

Single-molecule fluorescence spectroscopy has become a key methodology for the investigation of biomolecular mechanisms. A particular strength is the possibility to extract information on complex kinetics and dynamics over a broad range of timescales, both in equilibrium and non-equilibrium experiments[1-5]. Perturbation techniques are required in cases where the molecular species of interest are not populated to a detectable degree at equilibrium. Microfluidic mixing coupled to single-molecule detection is a powerful technique for investigating such biomolecular processes under non-equilibrium conditions[6-9], with dead times in the low millisecond range[7, 9] or even below[8]. A promising extension of rapid mixing is the double-jump mixing technique, which is well established for ensemble experiments based on stopped-flow mixing[10,11]: by enabling the transient population of unstable reaction intermediates, it allows their role in kinetic mechanisms to be probed. However, no such approach has been available for investigating kinetics with single-molecule resolution. Here we present a microfluidic device that is optimized for performing two consecutive rapid mixing steps separated by a well-defined delay time. In this way, a first change in solution conditions is employed to populate an unstable intermediate species, and a second mixing step to probe its kinetic properties. We demonstrate the versatility of this double-jump device with two examples occurring on very different timescales: (i) the association and dissociation of a protein complex on the millisecond timescale in a single experiment, and (ii) the kinetic investigation of an intermediate state in the conformational reorganization of a pore-forming toxin from milliseconds to minutes.

The design of the device (Figure 1a) is based on laminar flow and diffusive mixing[12] and was optimized for the desired mixing ratios and flow velocities using 3D finite-element calculations (Figure S1). The first rapid mixing step with a dead time of ~10 ms is followed by a delay channel whose length is optimized for the formation of the intermediate of interest. After the second mixing step, two additional pairs of outlet channels perpendicular to the observation channel were introduced. The effect of the resulting diverted flow is twofold: (1) The flow is rapidly decelerated to velocities compatible with confocal single-molecule detection[13], thus decreasing the dead time to ~7 ms, and (2) the even slower flow in the wider side outlet channels enables observation times of up to 5 minutes (Figure 1b), thus enabling a broad range of timescales to be investigated in a single device. The conformational changes of the sample molecules can be followed by confocal detection at various positions along the observation channel or in the side outlet channels. To obtain reliable devices with stable flow patterns and highly reproducible mixing behavior, we use microfabrication based on reactive ion etching in silicon for producing device molds with high accuracy in the resulting structures, essential especially for the narrow channels that enable fast diffusive mixing with millisecond dead time (Figure 1c). Combined with replica molding in poly(dimethylsiloxane) (PDMS)[14], large numbers of devices can be generated with great reproducibility and precision (see *Materials and Methods*), as verified by scanning electron microscopy (Figure 1c and Figure S2). The PDMS devices were bonded to microscope cover glasses after plasma activation (Figure 1d) and interfaced with confocal single-molecule detection via a previously described cartridge-based device holder[9]. Extensive testing of the flow patterns by wide-field fluorescence imaging (Figure S3) and of flow velocities and mixing ratios by fluorescence correlation spectroscopy (Figures S4 and S5) demonstrates good agreement with the results from finite-element calculations. To obtain an accurate conversion of positions along the observation channel to times after mixing, which is required for the quantitative kinetic analysis of the measurements[15], we carried out time-resolved finite-element calculations (Figure S6 and Video S1-S2).

We first demonstrate the performance of the microfluidic double-jump device for rapid processes on the millisecond timescale. To this end, we investigated the fast coupled folding and binding of the intrinsically disordered activation domain of the p160 transcriptional co-activator (ACTR) and the nuclear co-activator binding domain (NCBD) of CREB-binding protein[16], essential regulators of eukaryotic transcription[17]. In the first mixing step, ACTR labeled with Cy3B and LD650 as Förster resonance energy transfer (FRET) donor and acceptor, respectively, is delivered from the center inlet and mixed with an excess of unlabeled NCBD from the side inlets (100 nM initial concentration) to induce complex formation (Figure 2a). The following 5 mm-long channel serves as a delay line along which the two proteins have time to associate for 20 s. In the second mixing step, dissociation of the preformed complex is then triggered by dilution with buffer.

Figure 2b shows transfer efficiency histograms recorded after the first (left panel) and second mixing step (right panel), with the first histograms measured at 10 ms and 7 ms after mixing, respectively (Figures S7 and S8). To quantify the concentration dependence of this bimolecular reaction, the experiments were repeated with initial NCBD concentrations of 200 and 400 nM NCBD. A global kinetic analysis of all three datasets (Figure 2c) yields a dissociation rate coefficient of $7.1 \pm 0.4\ s^{-1}$ and an association rate coefficient of $0.6 \pm 0.2\ nM^{-1}s^{-1}$ (see *Materials and Methods* and Figure S9 for

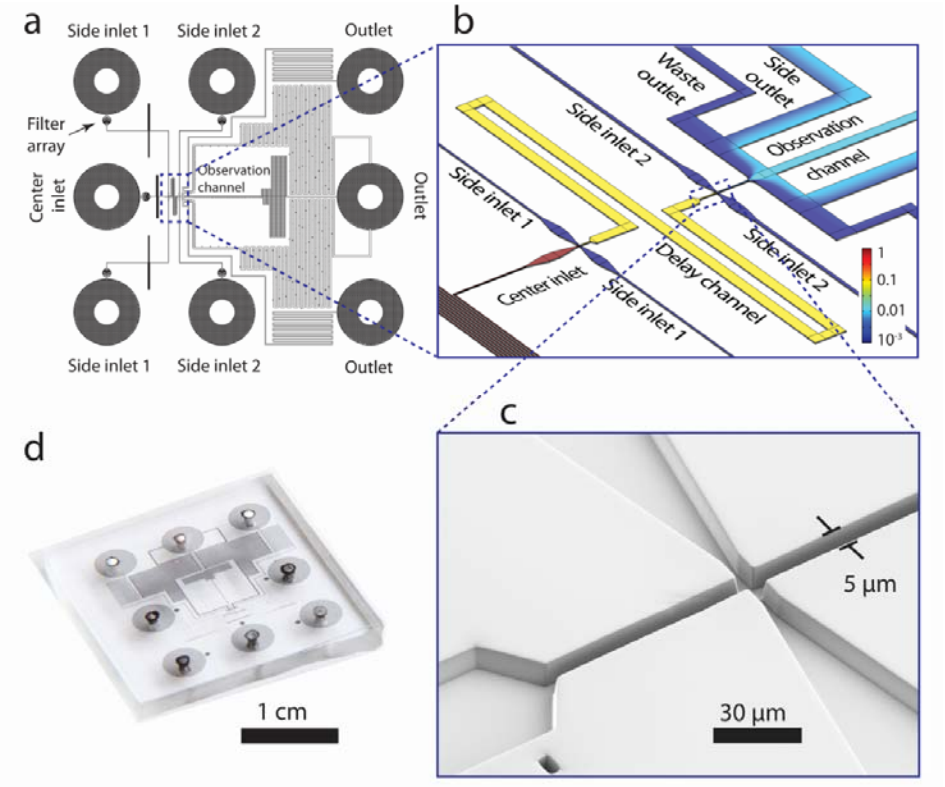

Figure 1. Design of the microfluidic double-jump mixing device. (a) and (b) Layout of the device: Solutes for the first mixing step are introduced from side inlets 1 (top and bottom) and mixed with the sample molecules from the center inlet. After passing a delay channel that defines the time between the two mixing steps, the sample is diluted by mixing with solutes from side inlets 2 (top and bottom). Microstructured filter arrays[9] were incorporated after each inlet to prevent obstruction of the channels by traces of dust. The relaxation to equilibrium can be followed by measuring at different positions along the observation channel, as each position corresponds to a different time after mixing. To rapidly decelerate the flow and to have access to longer timescales (up to ~5 min) additional outlet channels perpendicular to the observation channel are included. A typical calculated concentration profile of sample molecules ($D=10^{-10}$ m^2/s) introduced via the center inlet is shown in (b). Relative concentrations are plotted on a logarithmic scale, with the initial relative sample concentration set to 1. Note that while the mixing of small solutes is completed after the first and second mixing steps, respectively (Figure S1), the sample molecules are not uniformly distributed after the second mixing step because of their smaller diffusion coefficient. The partitioning into waste and side outlets ensures that the sample concentration in the side outlets is high enough for data recording. (c) Scanning electron micrograph of the second mixing region in the PDMS device to illustrate the high quality of the structures. (d) Photograph of the microfluidic device. For visualization, the microchannels are filled with ink.

details), in agreement with previous stopped-flow results[18]. By fabricating devices with different lengths of the delay channel, we can interrogate the effect of the association time on the dissociation kinetics. In the present case, reducing the association time to 25 ms (corresponding to a 87-µm delay channel) yields identical dissociation rate coefficients (Figure S10), indicating the absence of long-lived kinetic intermediates during complex formation.

To illustrate the suitability of the device for resolving more complex conformational changes in biomolecules over a broad range of timescales, we investigate a recently identified transient intermediate in the conformational transition of the pore-forming toxin ClyA[19]. ClyA is expressed as a soluble monomer that, upon interaction with membranes or detergent, undergoes a large conformational rearrangement into its protomer conformation[20]. This monomer-to-protomer transition involves a kinetic intermediate that is denatured and expanded[19]. However, owing to its transient nature, the properties of this intermediate have largely remained elusive. Here we use the microfluidic double-jump device to first form the intermediate state of ClyA by mixing the FRET-labeled protein with the membrane-mimicking detergent n-Dodecyl-β-D-Maltopyranoside (DDM) (Figure 3a); after 20 s in the delay channel, the low-FRET (i.e. rather expanded) intermediate is maximally populated. In the second mixing step, the protein is stripped of detergent by rapid mixing with β-cyclodextrin, a cyclic oligosaccharide that efficiently sequesters detergent molecules[21] (Figure S11). The second jump enables us to return to the initial solution conditions and investigate whether and how the intermediate of ClyA returns to the initial monomeric conformation.

Within the dead time of the measurement after the second mixing step, a broad transfer efficiency distribution with an average of $\langle E \rangle \approx 0.61$ is formed (Figure 3b), corresponding to a rapid collapse of the polypeptide chain. The pronounced broadening beyond the shot noise width is indicative of slow dynamics within the resulting conformational distribution[5, 22-23]. Only on a much longer timescale

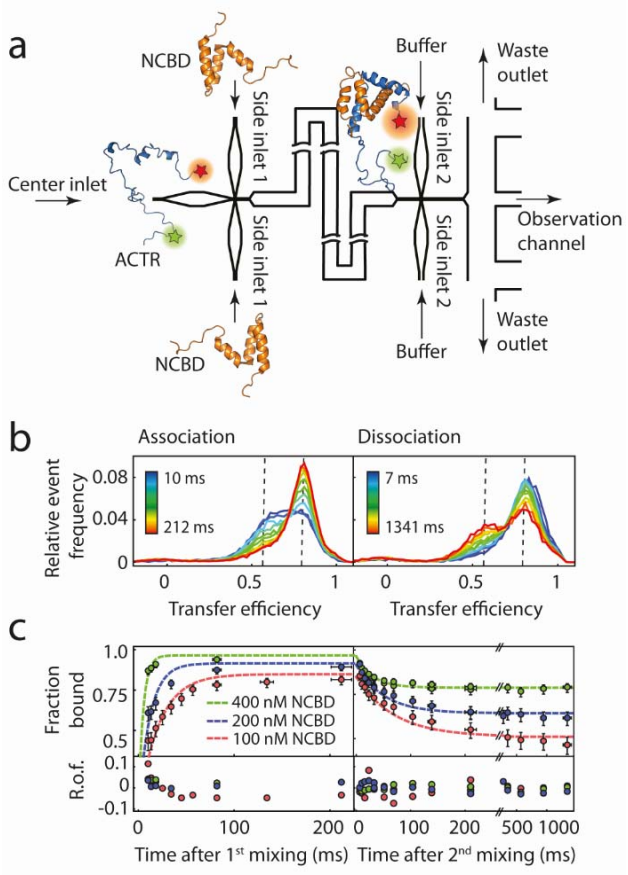

Figure 2. Coupled folding and binding of the intrinsically disordered proteins ACTR and NCBD investigated with the double-jump mixing device. (a) Donor- and acceptor-labeled ACTR is mixed in the first step with an excess of unlabeled NCBD to induce complex formation. Dissociation is triggered in the second mixing step by dilution with buffer solution. (b) Transfer efficiency histograms measured at various positions along the channels after the first and second mixing steps (left and right panel, respectively; normalized to an area of 1), corresponding to different times after the start of the reaction (as indicated by the color scale). The low transfer efficiency peak, $\langle E \rangle \approx 0.60$, corresponds to free ACTR and the high transfer efficiency peak, $\langle E \rangle \approx 0.80$, to folded ACTR within the complex with NCBD (100 nM initial concentration). (c) Global fit (dashed colored lines) of the association (left) and dissociation kinetics (right) for three different initial NCBD concentrations (100, 200 and 400 nM). The error bars indicate the uncertainties from fitting the transfer efficiency histograms.

of 5±1 s, a transition takes place to a population with a transfer efficiency of ~0.43, characteristic of the known folded monomer conformation[19] (Figure 3c-d, Figures. S12-S13 and Table S1). Further narrowing of the transfer efficiency distribution is observed by measurements in the additional observation channel up to 4.5 min after mixing (Figure S14). Full conversion to the narrow histogram of the monomer, however, is only complete after ~10 min, as revealed by manual mixing experiments (Figure 3b), which can be combined with the longest timescales accessible in the mixer without any time gap. Overall, the results on ClyA illustrate the capacity of double-jump mixing to probe the behavior of complex kinetics and intermediates that would otherwise be inaccessible.

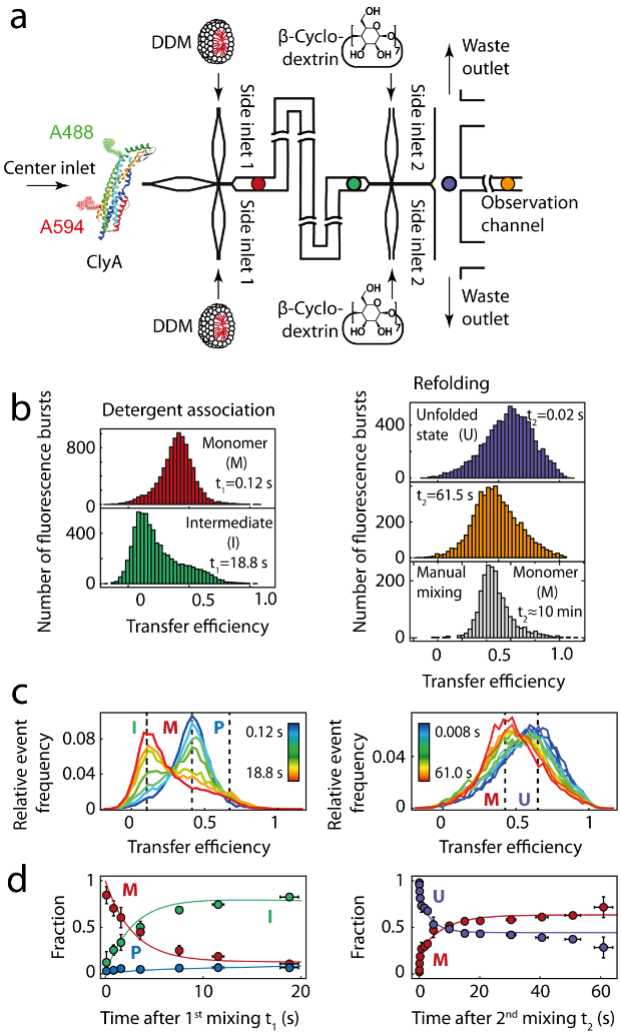

Figure 3. Probing the intermediate state of the pore-forming toxin ClyA by rapid double-jump mixing. (a) Schematic of the measure ment. (b) Transfer efficiency histograms measured at different positions in the device (indicated by corresponding colored circles in (a)) reveal different ClyA conformations. Mixing of ClyA in its monomer conformation (M) with n-dodecyl β-D-maltopyranoside (DDM, 0.11 % w/v) induces the formation of a denatured intermediate state (I). After maximally populating I in the delay channel, the protein is stripped of detergent by addition of the cyclic oligosaccharide β-cyclodextrin (0.058 % w/v) in the second mixing step, which causes a collapse of I to the compact unfolded state U. Within ~1 min, ClyA returns to the average transfer efficiency of M. In manual mixing experiments (lowest panel on the right), complete conversion to the narrow transfer efficiency distribution of the monomer is observed. (c) Normalized transfer efficiency histogram time series indicating the time-course of the transition from M ($\langle E \rangle = 0.42$) to I ($\langle E \rangle = 0.13$) after the first mixing step (left), and from U ($\langle E \rangle = 0.61$) to M ($\langle E \rangle = 0.43$) after the second mixing step (right). The transition from I to U occurs within the dead time (7 ms). (d) Left panel: Fractions of monomer (M), intermediate (I) and protomer (P) after the first mixing step obtained from a global fit of the histograms (colored circles), overlaid with a kinetic off-pathway model using previously described rates[19] (lines). Right panel: Fractions of M and U after the second mixing step fitted with a biexponential fit (for M: τ_1=0.2±0.1 s, 36% of total amplitude, and τ_2=8.0±1.9 s, 64% of total amplitude) (see *Materials and Methods* for details).

In summary, we present here a microfluidic device for rapid double-jump mixing experiments in combination with single-molecule spectroscopy, with observation times from milliseconds to minutes after mixing. The approach combines the advantages of non-equilibrium perturbation techniques with the ability of single-molecule spectroscopy to resolve conformational heterogeneity. The technique is particularly valuable for probing transiently populated states that are neither accessible at equilibrium nor in single-step-mixing experiments. The device thus enables the discovery of elusive transient species in biomolecular mechanisms and provides a powerful extension of the single-molecule toolbox.

ASSOCIATED CONTENT

Supporting Information

The Supporting Information is available free of charge on the ACS Publications website at DOI:

Materials and methods section and additional figures (PDF)

Videos of the time-resolved finite element calculations (avi)

AUTHOR INFORMATION

Corresponding Author

[#]schuler@bioc.uzh.ch

Notes

The authors declare no competing financial interests.

ACKNOWLEDGMENT

We thank Scott Blanchard for the generous gift of LD650 maleimide. We thank Donat Scheiwiller, Stefan Blunier (Institute of Mechanical Systems, ETH Zurich), and Vincent Romain Joseph Martinez for help with microfabrication; the Center for Microscopy and Image Analysis (University of Zurich) for assistance and support with scanning electron microscopy; Adrian Schmid and Sascha Weidner for technical assistance; Hagen Hofmann and Karin Buholzer for providing an expression plasmid for ACTR and NCBD; Jendrik Schöppe and Andreas Plückthun for providing the pAT222-pD vector, and Ruth Kellner for the photographs of the microfluidic device. This work was supported by the Swiss National Science Foundation (B.S.) and by a postdoctoral fellowship from the Forschungskredit of the University of Zurich (N.Z.).

REFERENCES

(1) Selvin, P. R.; Ha, T., *Single-molecule techniques: A laboratory manual*. Cold Spring Harbor Laboratory Press: New York, 2008.

(2) Schuler, B.; Hofmann, H., *Curr. Opin. Struct. Biol.* **2013,** *23*, 36.

(3) Holmstrom, E. D.; Nesbitt, D. J., *Annu. Rev. Phys. Chem.* **2016,** *67*, 441.

(4) Rigler, R.; Elson, E. S., *Flourescence correlation spectroscopy: Theory and applications*. Springer: Berlin, 2001.

(5) Gopich, I. V.; Szabo, A., Theory of single-molecule FRET efficiency histograms. In *Single-molecule biophysics: experiment and theory, Vol 146*, Komatsuzaki, T.; Kawakami, M.; Takahashi, S.; Yang, H.; Silbey, R. J., Eds. 2012; 245.

(6) Lipman, E. A.; Schuler, B.; Bakajin, O.; Eaton, W. A., *Science* **2003,** *301*, 1233.

(7) Pfeil, S. H.; Wickersham, C. E.; Hoffmann, A.; Lipman, E. A., *Rev. Sci. Instrum.* **2009,** *80*, 055105.

(8) Gambin, Y.; VanDelinder, V.; Ferreon, A. C. M.; Lemke, E. A.; Groisman, A.; Deniz, A. A., *Nat. Methods* **2011,** *8*, 239.

(9) Wunderlich, B.; Nettels, D.; Benke, S.; Clark, J.; Weidner, S.; Hofmann, H.; Pfeil, S. H.; Schuler, B., *Nat. Protocols* **2013,** *8*, 1459.

(10) Welker, E.; Maki, K.; Shastry, M. C. R.; Juminaga, D.; Bhat, R.; Scheraga, H. A.; Roder, H., *Proc. Natl. Acad. Sci. USA* **2004,** *101*, 17681.

(11) Krantz, B. A.; Sosnick, T. R., *Biochemistry* **2000,** *39*, 11696.

(12) Knight, J. B.; Vishwanath, A.; Brody, J. P.; Austin, R. H., *Phys. Rev. Lett.* **1998,** *80*, 3863.

(13) Gambin, Y.; Simonnet, C.; VanDelinder, V.; Deniz, A.; Groisman, A., *Lab Chip* **2010,** *10*, 598.

(14) Duffy, D. C.; McDonald, J. C.; Schueller, O. J. A.; Whitesides, G. M., *Anal. Chem.* **1998,** *70*, 4974.

(15) Wunderlich, B.; Nettels, D.; Schuler, B., *Lab Chip* **2014,** *14*, 219.

(16) Dogan, J.; Schmidt, T.; Mu, X.; Engström, Å.; Jemth, P., *J. Biol. Chem.* **2012,** *287*, 34316.

(17) Dyson, H. J.; Wright, P. E., *J. Biol. Chem.* **2016,** *291*, 6714.

(18) Dogan, J.; Jonasson, J.; Andersson, E.; Jemth, P., *Biochemistry* **2015,** *54*, 4741.

(19) Benke, S.; Roderer, D.; Wunderlich, B.; Nettels, D.; Glockshuber, R.; Schuler, B., *Nat. Commun.* **2015,** *6*, 6198.

(20) Mueller, M.; Grauschopf, U.; Maier, T.; Glockshuber, R.; Ban, N., *Nature* **2009,** *459*, 726.

(21) Otzen, D. E.; Oliveberg, M., *J. Mol. Biol.* **2001,** *313*, 479.

(22) Kalinin, S.; Valeri, A.; Antonik, M.; Felekyan, S.; Seidel, C. A., *J. Phys. Chem. B* **2010,** *114*, 7983.

(23) Nir, E.; Michalet, X.; Hamadani, K. M.; Laurence, T. A.; Neuhauser, D.; Kovchegov, Y.; Weiss, S., *J. Phys. Chem. B* **2006,** *110*, 22103.

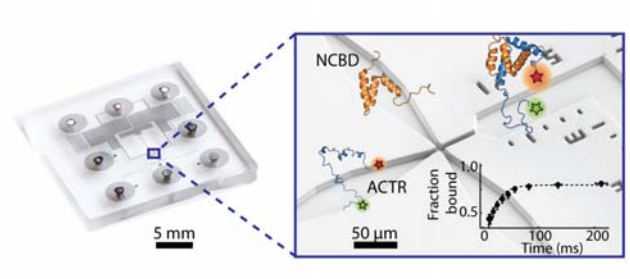
NCBD
ACTR
5 mm
50 µm
Fraction bound
1.0
0.5
0
100
200
Time (ms)